Supporting Information

To

Suppression of Hydrogen Evolution in Acidic Electrolytes by Electrochemical CO_2 Reduction

Christoph J. Bondue[a], Matthias Graf [a,b], Akansha Goyal[a] and Marc T. M. Koper[a] *

[a] Leiden Institute of Chemistry, Leiden University, P.O. Box 9502, 2300 RA Leiden, The Netherlands.

[b] Institute for Materials Research, Helmholtz Center Geesthacht, Max-Planck-Str. 1, 21502 Geesthacht, Germany.

1. Effect of Proton Concentration on Hydrogen Evolution and CO_2-Reduction

Figures S1, S2 and S3 show the DEMS data presented in Figure 1 and those obtained for electrolytes featuring proton concentrations of 0.63 mM, 0.4 mM and 0.25 mM converted into the partial faradaic current due to hydrogen evolution and the partial faradaic current due to CO-formation. For all proton concentrations, the formation rate of CO increases when the partial pressure of CO_2 in the Ar/CO-mixture increases. In all measurements a trend to a somewhat larger CO formation rate is observed when the proton concentration is increased.

At -0.85 V vs Ag|AgCl the formation rate of hydrogen increases linearly with the proton concentration, which is expected when proton reduction reaches diffusion limitation. Once CO_2 reduction sets in, the current due to proton reduction decreases in the same fashion as discussed in Figure 1 and reaches a minimum at around -1.28 V vs Ag|AgCl. This minimum is smallest when the CO formation rate is highest and the proton concentration lowest. At potentials lower than -1.4 V vs Ag|AgCl, hydrogen evolution due to water reduction sets in. This process is not enhanced when the proton concentration is higher.

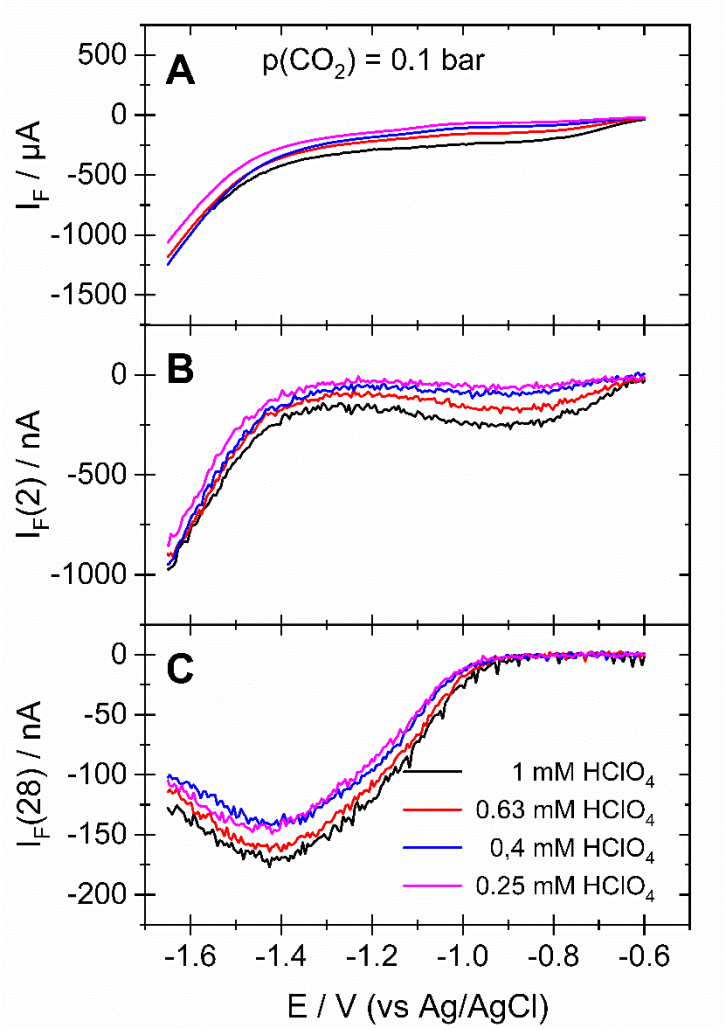

Figure S1: DEMS-data (cathodic sweep only) for an experiment in which the electrolyte of 0.5 M $NaClO_4$ containing different concentrations of $HClO_4$ was purged with an Ar/CO_2-mixture featuring a CO_2 partial pressure of 0.1 bar: $HClO_4$-contentration: 1 mM (black); 0.63 mM (red); 0.4 mM (blue); 0.25 mM (magenta). A: measured faradaic current as a function of the potential; B: partial faradaic current due to hydrogen evolution determined from the measured ionic current for mass 2; C: partial faradaic current for the evolution of CO determined from the measured ionic current for mass 28. Working electrode: polycrystalline gold electrode with a roughness factor of 20.3; sweep rate: 20 mV/s; Flow rate: 5 µL/s; Exposed geometric surface area: 0.283 cm^2.

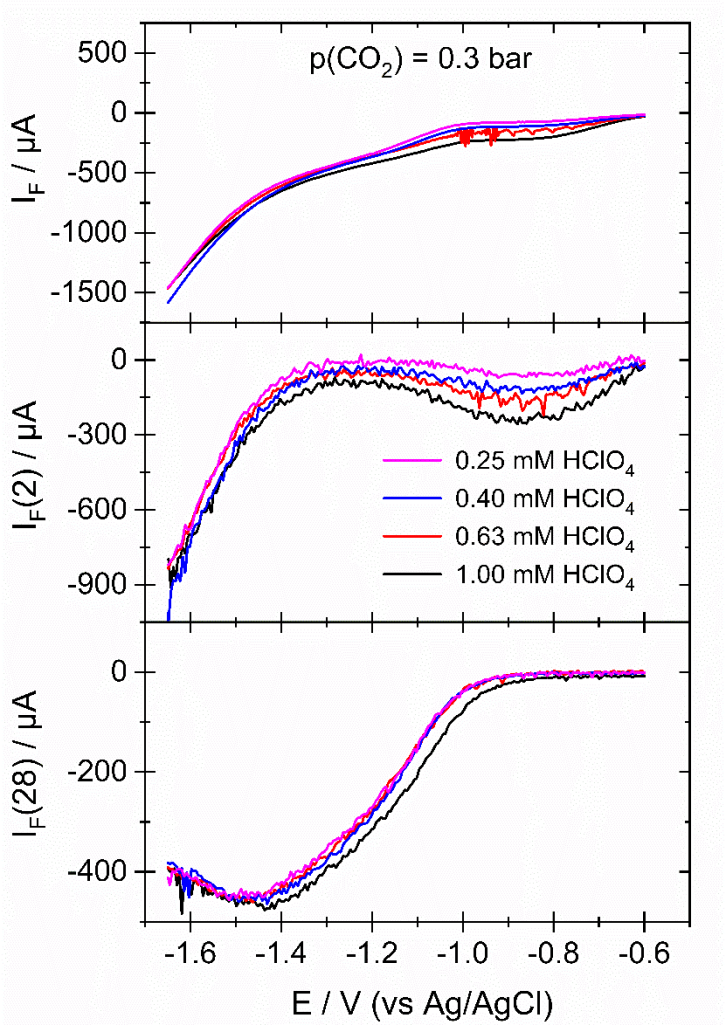

Figure S2: DEMS-data (cathodic sweep only) for an experiment in which the electrolyte of 0.5 M $NaClO_4$ containing different concentrations of $HClO_4$ was purged with an Ar/CO_2-mixture featuring a CO_2 partial pressure of 0.3 bar: $HClO_4$-contentration: 1 mM (black); 0.63 mM (red); 0.4 mM (blue); 0.25 mM (magenta). A: measured faradaic current as a function of the potential; B: partial faradaic current due to hydrogen evolution determined from the measured ionic current for mass 2; C: partial faradaic current for the evolution of CO determined from the measured ionic current for mass 28. Working electrode: polycrystalline gold electrode with a roughness factor of 20.3; sweep rate: 20 mV/s; Flow rate: 5 µL/s; Exposed geometric surface area: 0.283 cm².

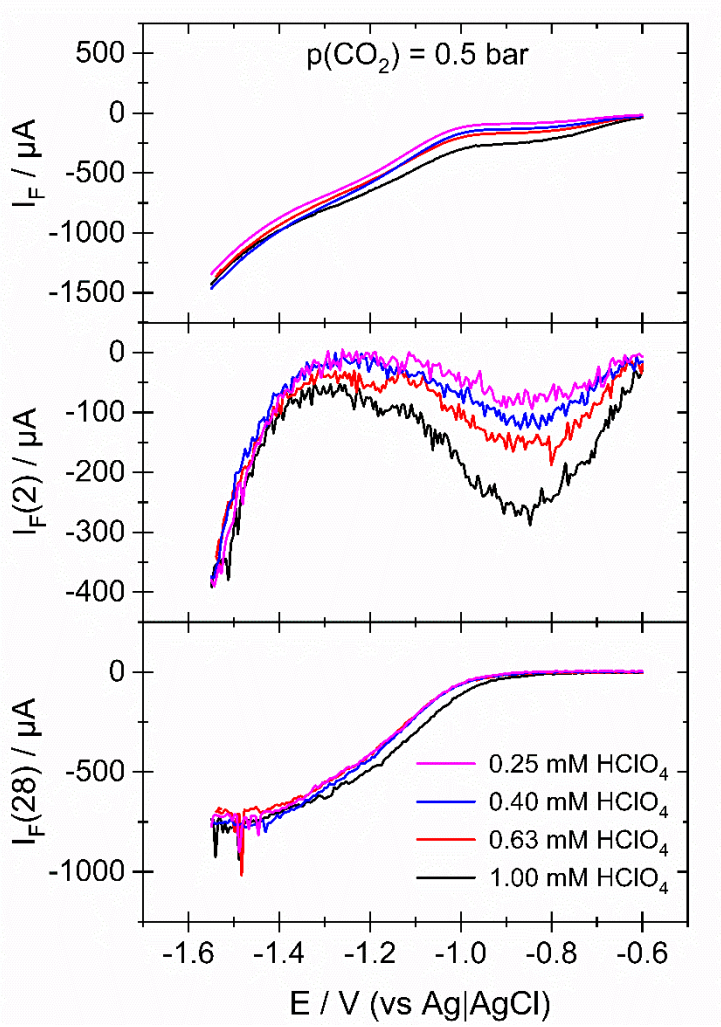

Figure S3: DEMS-data (cathodic sweep only) for an experiment in which the electrolyte of 0.5 M $NaClO_4$ containing different concentrations of $HClO_4$ was purged with an Ar/CO_2-mixture featuring a CO_2 partial pressure of 0.3 bar: $HClO_4$-contentration: 1 mM (black); 0.63 mM (red); 0.4 mM (blue); 0.25 mM (magenta). A: measured faradaic current as a function of the potential; B: partial faradaic current due to hydrogen evolution determined from the measured ionic current for mass 2; C: partial faradaic current for the evolution of CO determined from the measured ionic current for mass 28. Working electrode: polycrystalline gold electrode with a roughness factor of 20.3; sweep rate: 20 mV/s; Flow rate: 5 µL/s; Exposed geometric surface area: 0.283 cm².

2. Effect of Electrode Roughness Factor on the Rate of Hydrogen Evolution and CO_2-Reduction

Figure S4 shows the same experiment as shown in Figure 1 in the main text conducted with a gold electrode with a roughness factor of 2.8. In Figure S4 the CV can be reproduced again from the ionic currents for masses 2 and 28. As expected, onset potentials and signal shapes are not affected by the electrode roughness. However, Figures S4G, S4H and S4I show that the formation rate of CO is lower at the smooth electrode. As discussed in the main text the formation rate of CO is limited by the reaction kinetics and declines therefore with the real surface area.

In the potential range of proton reduction, the rate of hydrogen evolution increases when the roughness factor is reduced. As shown in Figure 2 proton reduction enters diffusion limitation at potentials lower -0.95 V vs Ag|AgCl. However, mass transport of protons to the electrode surfaces only depends on the geometric surface area. Hence, the same amount of protons is available to support an electrochemical reaction at the electrode surface. Since the rate of CO_2-reduction is lower, fewer protons are needed to support CO formation. Hence, more protons are available for the electrochemical evolution of hydrogen.

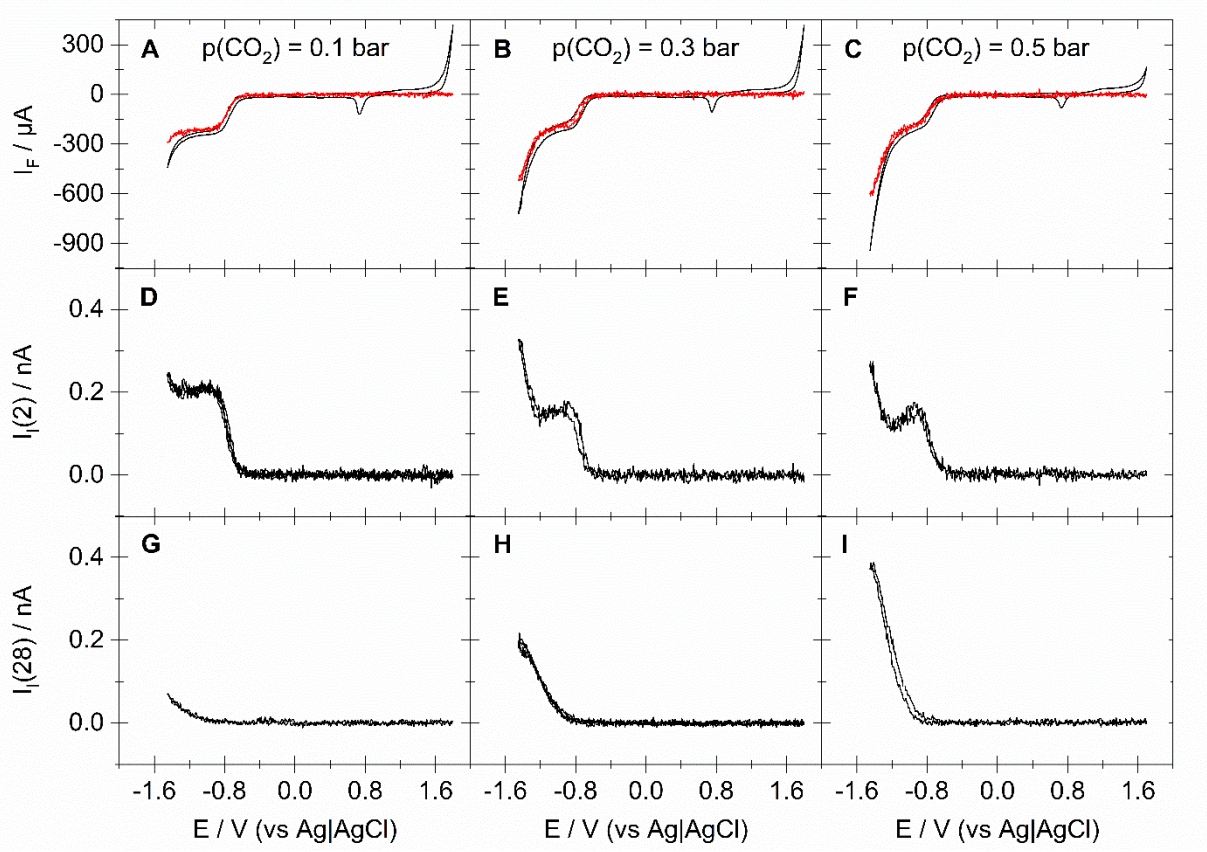

Figure S4: DEMS-data for the electrochemical CO_2-reduction at a polycrystalline gold electrode with a roughness factor of 2.8 (exposed geometric surface: area 0.283 cm^2). A, B and C: Measured CV (black) and CV predicted from the amounts of evolved H_2 and CO (red); D, E and F: ionic current for mass 2 corresponding to the CVs in A, B and C, respectively; G, H and I: ionic current for mass 2 corresponding to the CVs in A, B and C, respectively; Electrolyte: 0.5 M $NaClO_4$ containing 1 mM $HClO_4$ purged with Ar/CO_2-mixtures featuring different CO_2 partial pressures: 0.1 bar (A, D and G), 0.3 bar (B, E and H) and 0.5 bar (C, F and I). Sweep rate: 20 mV/s; Flow rate: 5 µL/s.

Figure S5 shows the Faradaic Efficiency of CO_2 reduction to CO at a smooth gold electrode. The plotted Faradaic Efficiency was determined from the experimental data shown in Figure S4. Because of the higher formation rate of hydrogen and the lower formation rate of CO, the Faradaic Efficiency of CO_2 reduction shown in Figure S5 is lower than that obtained at the roughened electrode (c.f. Figure S4). As in Figure 3, the Faradaic Efficiency of CO formation goes through a maximum when the partial pressure of CO2 is 0.3 bar and 0.5 bar. However, no maximum is observed in the investigated potential range for a CO_2 partial pressure of 0.1 bar. The maxima in the black and blue curve of Figure S5 coincide

with the onset of water reduction in Figure S4. Since water reduction is not yet very prominent at the reverse potential in Figure S4, no maximum is observed in the red curve of Figure S5.

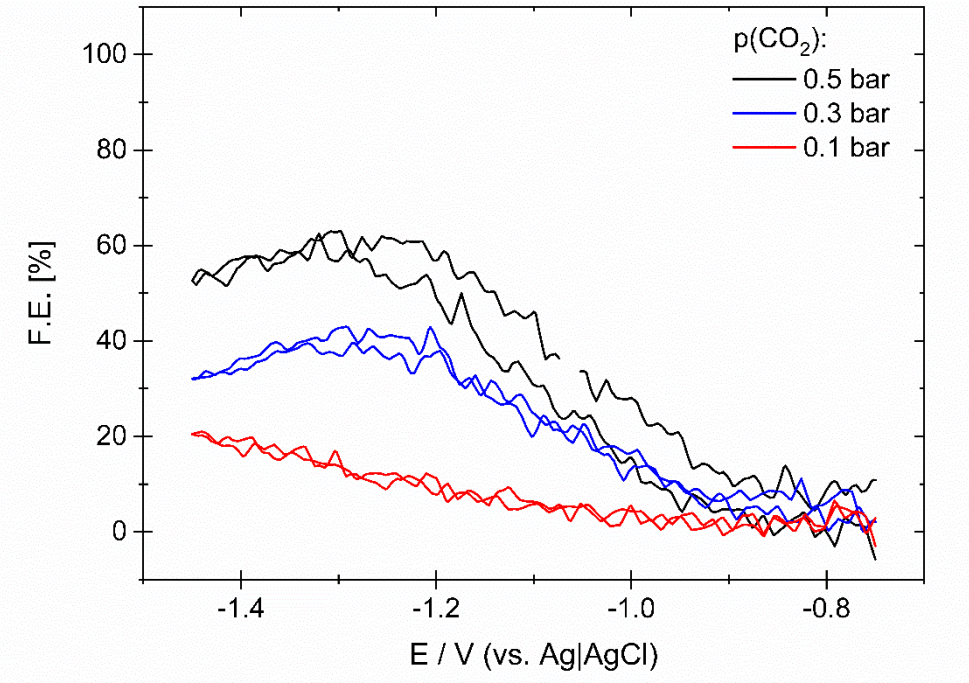

Figure S5: Faradaic Efficiency of CO_2 reduction at a polycrystalline gold electrode with a roughness factor of 2.8. The electrolyte was an aqueous solution of 0.5 M $NaClO_4$ containing 1mM $HClO_4$. The electrolyte was purged with Ar/CO_2-mixtures featuring different CO_2 partial pressures: 0.1 bar (red), 0.3 bar (blue) and 0.5 bar (black). Sweep rate: 20 mV/s; Flow rate: 5 µL/s. The corresponding DEMS data from which the Faradaic Efficiency was calculated are shown in Figure S4.

3. Mass balance of Hydrogen and Carbon

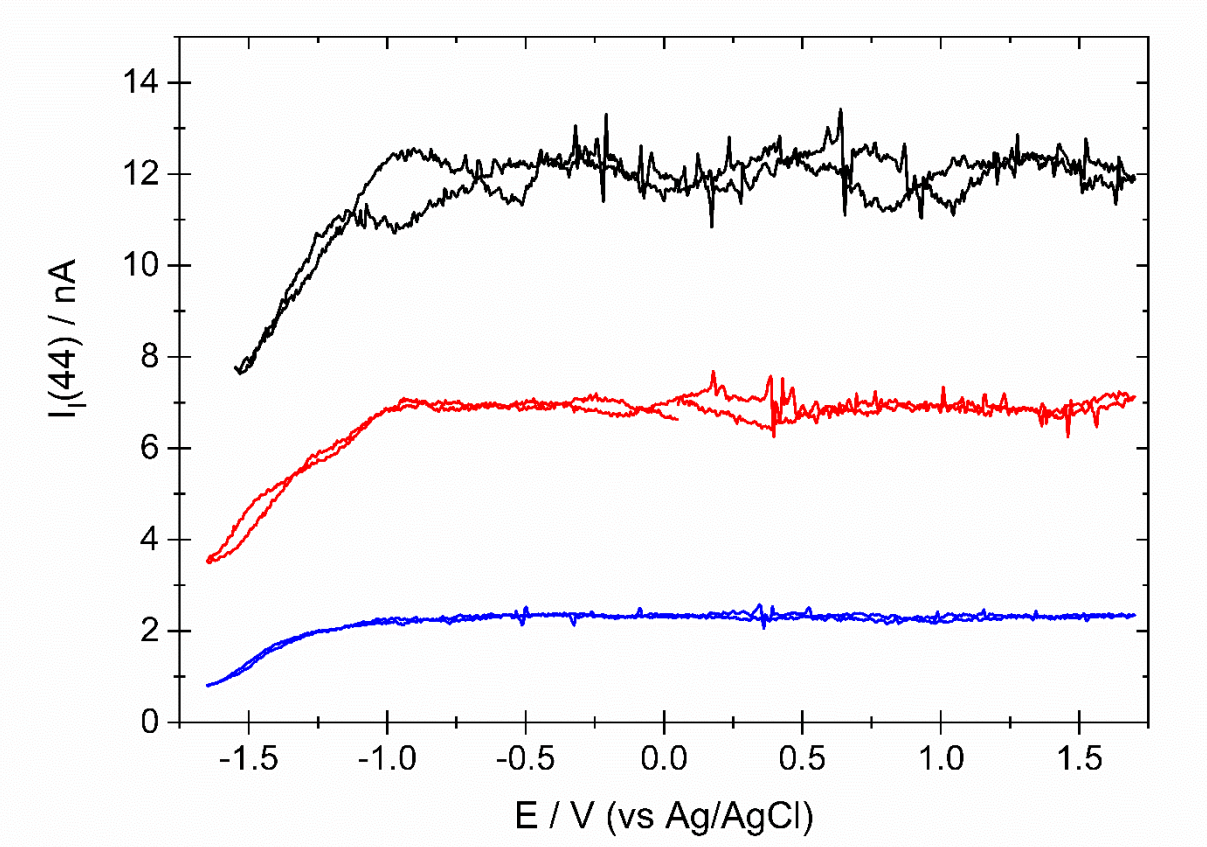

Figure S6: ionic current for mass 44 during CO_2 reduction when an electrolyte of 0.5 M $NaClO_4$ + 1mM $HClO_4$ was purged with an Ar/CO_2-mixture featuring a CO_2-partial pressure of 0.5 bar (black), 0.3 bar (red) and 0.1 bar (blue), respectively. Working electrode: Au(pc) (roughness factor: 20.3; exposed geometric surface: area 0.283 cm^2); Sweep rate: 20 mV/s; Flow rate: 5 µL/s.

Figure S6 shows the ionic current for mass 44 recorded parallel to the data presented in Figure 1. At around -0.95 V vs Ag|AgCl the ionic current for mass 44 begins to decrease from its baseline value. After calibration and baseline correction, we can determine from these data the flux of CO_2 ($F(CO_2)$) that is consumed during CO_2 reduction. These data are shown in Figures S7, S8 and S9 for electrolytes with a proton concentration of 0.63 mM, 0.4 mM and 0.25 mM, respectively. These figures also show $F_{CO2}(CO)$, $F_{CO2}(H^+)$, D_{H+} and S_{CO2}, which display the same behavior as in Figure 4.

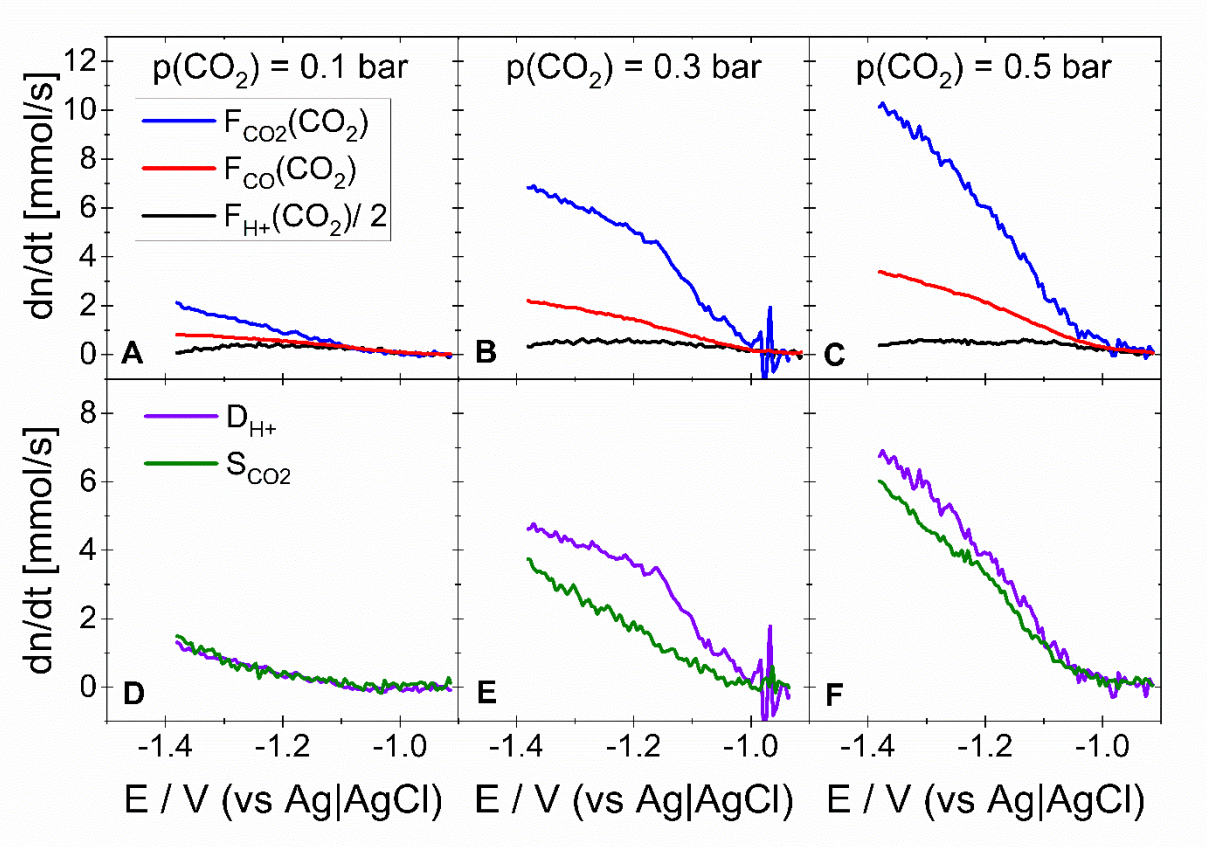

Figure S7: Top panels: Flux of protons divided by 2 (black), of CO_2 (blue) and of CO (red) that are consumed and produced during CO_2 reduction, respectively. Bottom panels: Proton deficit (violet) and CO_2 surplus (olive). The electrolyte was 0.5 M $NaClO_4$ + 0.63 mM $HClO_4$ purged with an Ar/CO_2-gas mixture featuring a CO_2 partial pressure of 0.1 bar (A and D), 0.3 bar (B and E) and 0.5 bar (C and F). Working electrode: Au(pc) (roughness factor: 20.3; exposed geometric surface: area 0.283 cm^2); Sweep rate: 20 mV/s; Flow rate: 5 µL/s.

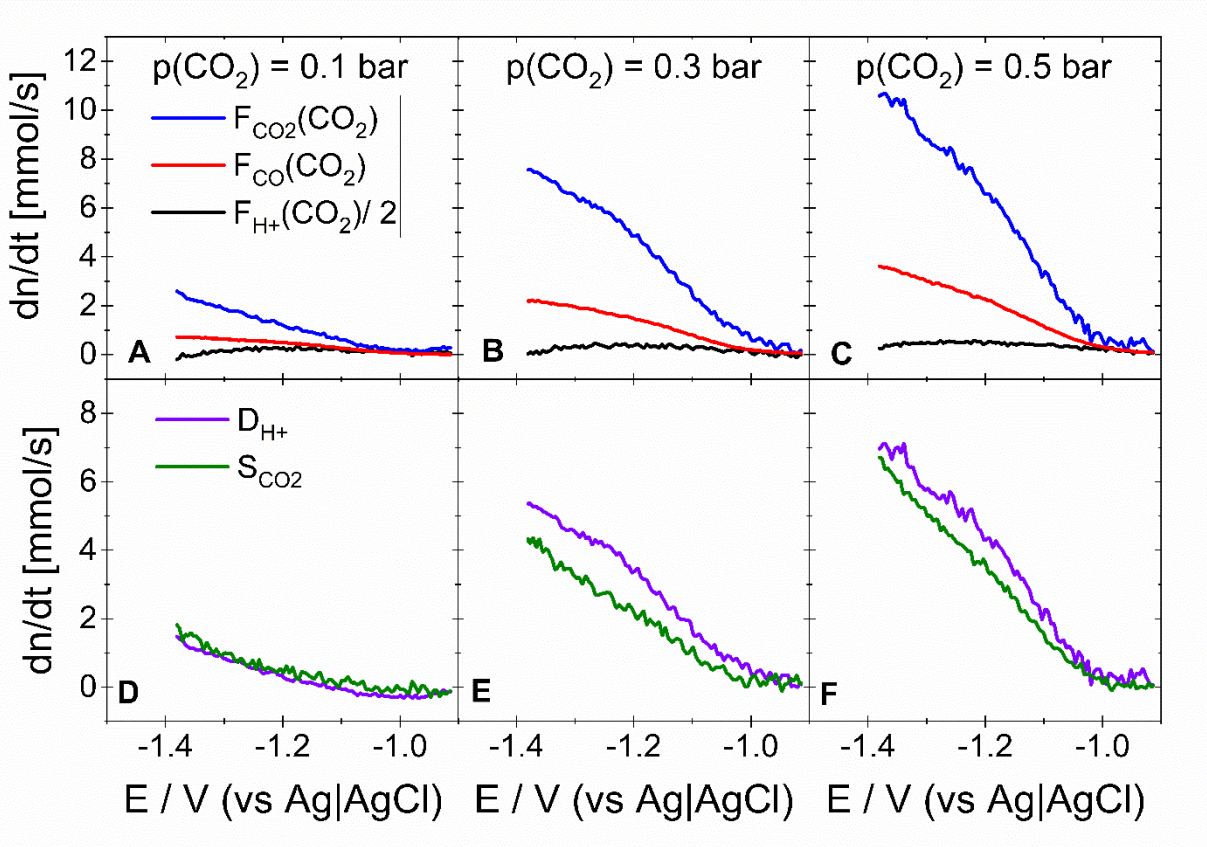

Figure S8: Top panels: Flux of protons divided by 2 (black), of CO_2 (blue) and of CO (red) that are consumed and produced during CO_2 reduction, respectively. Bottom panels: Proton deficit (violet) and CO_2 surplus (olive). The electrolyte was 0.5 M $NaClO_4$ + 0.4 mM $HClO_4$ purged with an Ar/CO_2-gas mixture featuring a CO_2 partial pressure of 0.1 bar (A and D), 0.3 bar (B and E) and 0.5 bar (C and F). Working electrode: Au(pc) (roughness factor: 20.3; exposed geometric surface: area 0.283 cm^2); Sweep rate: 20 mV/s; Flow rate: 5 µL/s.

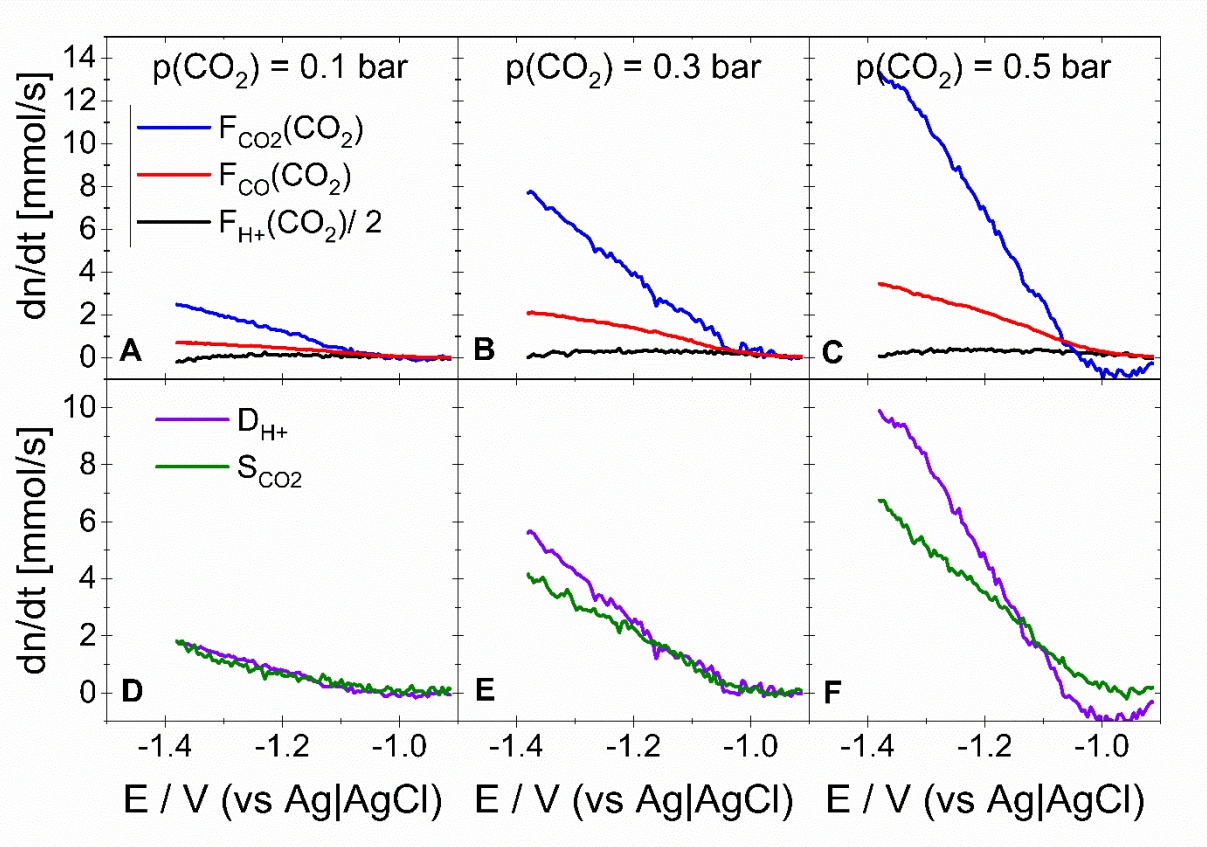

Figure S9: Top panels: Flux of protons divided by 2 (black), of CO_2 (blue) and of CO (red) that are consumed and produced during CO_2 reduction, respectively. Bottom panels: Proton deficit (violet) and CO_2 surplus (olive). The electrolyte was 0.5 M $NaClO_4$ + 0.25 mM $HClO_4$ purged with an Ar/CO_2-gas mixture featuring a CO_2 partial pressure of 0.1 bar (A and D), 0.3 bar (B and E) and 0.5 bar (C and F). Working electrode: Au(pc) (roughness factor: 20.3; exposed geometric surface: area 0.283 cm²); Sweep rate: 20 mV/s; Flow rate: 5 µL/s.

According to Reaction 2a in the main paper, reduction of one molecule of CO_2 results in the formation of 2 OH^- ions. The formation rate of OH^- is $F_{CO2}(OH^-)$ is twice the formation rate of CO (Equation S1) and twice the flux $F_{CO2}(CO_2)$ of CO_2 that is reduced to CO.

$$F_{CO2}(OH^-) \quad = 2 \cdot F_{CO2}(CO) = 2 \cdot F_{CO2}(CO_2) \qquad \text{Eq. S1}$$

The generated OH^- forms water with the rate $F_{H2O}(OH^-)$ (Reaction 2 in the main paper) and with the rate $F_{HCO3-}(OH^-)$ bicarbonate (Reaction 7 in the main paper). $F_{H2O}(OH^-)$ equals the flux of protons that "participate" in CO_2 reduction (Equation S2), and $F_{HCO3-}(OH^-)$ equals the flux of CO_2 that participates in bicarbonate formation (Equation S3).

$$F_{CO2}(H^+) = F_{H2O}(OH^-) \quad \text{Eq. S2}$$

$$F_{HCO3-}(OH^-) = F_{HCO3-}(CO_2) \quad \text{Eq. S3}$$

The overall rate of CO_2 consumption $F(CO_2)$ (plotted in Figure 4, S7, S8 and S9) equals the sum of the rate of CO_2 leading to CO formation and the rate of bicarbonate formation (Equation S4a). Replacing $F_{CO2}(CO_2)$ with the CO formation rate and rearrangement of Equation S4a yields Equation S4b. Comparison of Equation S4b with Equation 6 in the main text shows that the rate of Reaction 7 in the main paper equals the surplus of CO_2 consumption S_{CO2}.

$$F(CO_2) = F_{HCO3-}(CO_2) + F_{CO2}(CO_2) \quad \text{Eq. S4a}$$

$$= F_{HCO3-}(CO_2) + F_{CO2}(CO)$$

$$F(CO_2) - F_{CO2}(CO) = F_{HCO3-}(CO_2) = S_{CO2} \quad \text{Eq. S4b}$$

The rate of OH^- formation via Reaction 1 must equal the rate of its consumption via Reaction 2 and 7 (Equation S5a). Rearrangement of Equation S5a and insertion of Equation S1, S2 and S3 yields Equation S5b, which shows that the flux of protons participating in CO_2 reduction equals twice the rate of CO formation minus the rate of bicarbonate formation.

$$F_{CO2}(OH^-) = F_{H2O}(OH^-) + F_{HCO3-}(OH^-) \quad \text{Eq. S5a}$$

$$F_{CO2}(H^+) = 2 \cdot F_{CO2}(CO) - F_{HCO3-}(CO_2) \quad \text{Eq. S5b}$$

4. CO_2 Partial Pressure at the Electrode Surface

Since CO_2 reacts increasingly off with OH^- formed either in the course of CO_2 reduction or during water reduction, its concentration in the vicinity of the electrode surfaces is increasingly reduced. We can estimate the partial pressure of CO_2 at the electrode surface $p_0(CO_2)$ from the monitored ionic current for mass 44 via Equation S6.

$$p_0(CO_2) = p(CO_2) \cdot \frac{I_I(44)}{I_{I,base}(44)} \qquad \text{Eq. S6}$$

In Equation S6 $I_I(44)$ represents the measured ionic current for mass 44, $I_{I,base}(44)$ is the baseline value of the ionic current for mass 44 determined in the potential range between 0.0 and -0.5 V vs Ag|AgCl and $p(CO_2)$ is the partial pressure of CO_2 in the Ar/CO_2 mixture with which the electrolyte is purged. Figures S10, S11 and S12 show that $p_0(CO_2)$ undergoes a drastic decline during the measurements that are presented in Figures S1, S2 and S3. In relative terms, this is particularly true for the electrolyte purged with an Ar/CO_2 mixture featuring a CO_2 partial pressure of 0.1 bar, where $p_0(CO_2)$ drops by 80% down to 0.02 bar. Accordingly, the CO formation rate decreases or stops to increase when during water reduction CO_2 reacts increasingly off with OH^-.

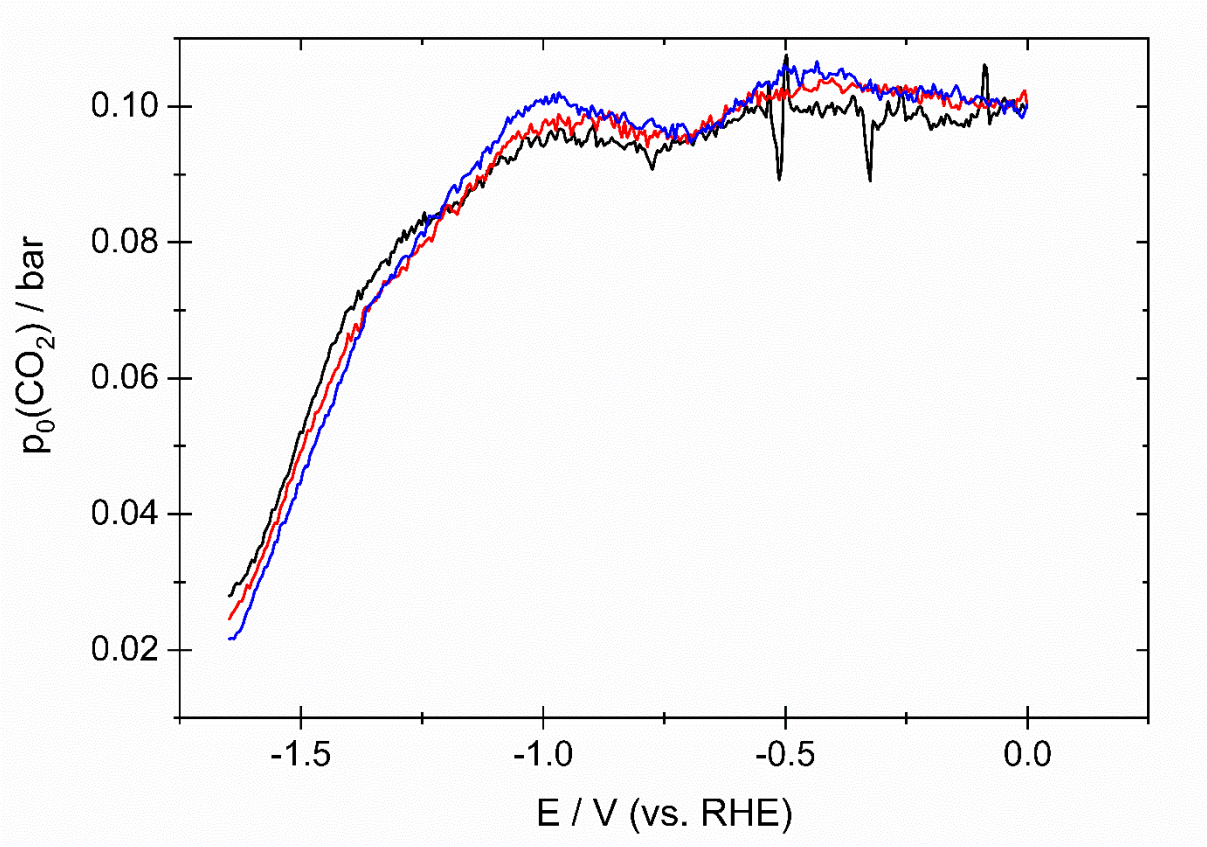

Figure S10: The CO_2 partial pressure at the electrode surface estimated from Equation S5 for the measurements shown in Figure S1. The electrolyte of 0.5 M $NaClO_4$ containing 1 mM (black), 0.63 mM (red), 0.4 mM (blue) and 0.25 mM (magenta) $HClO_4$ was purged with an Ar/CO_2 mixture featuring a CO_2 partial pressure of 0.1 bar. Working electrode: Au(pc) (roughness factor: 20.3; exposed geometric surface: area 0.283 cm^2); Sweep rate: 20 mV/s; Flow rate: 5 µL/s.

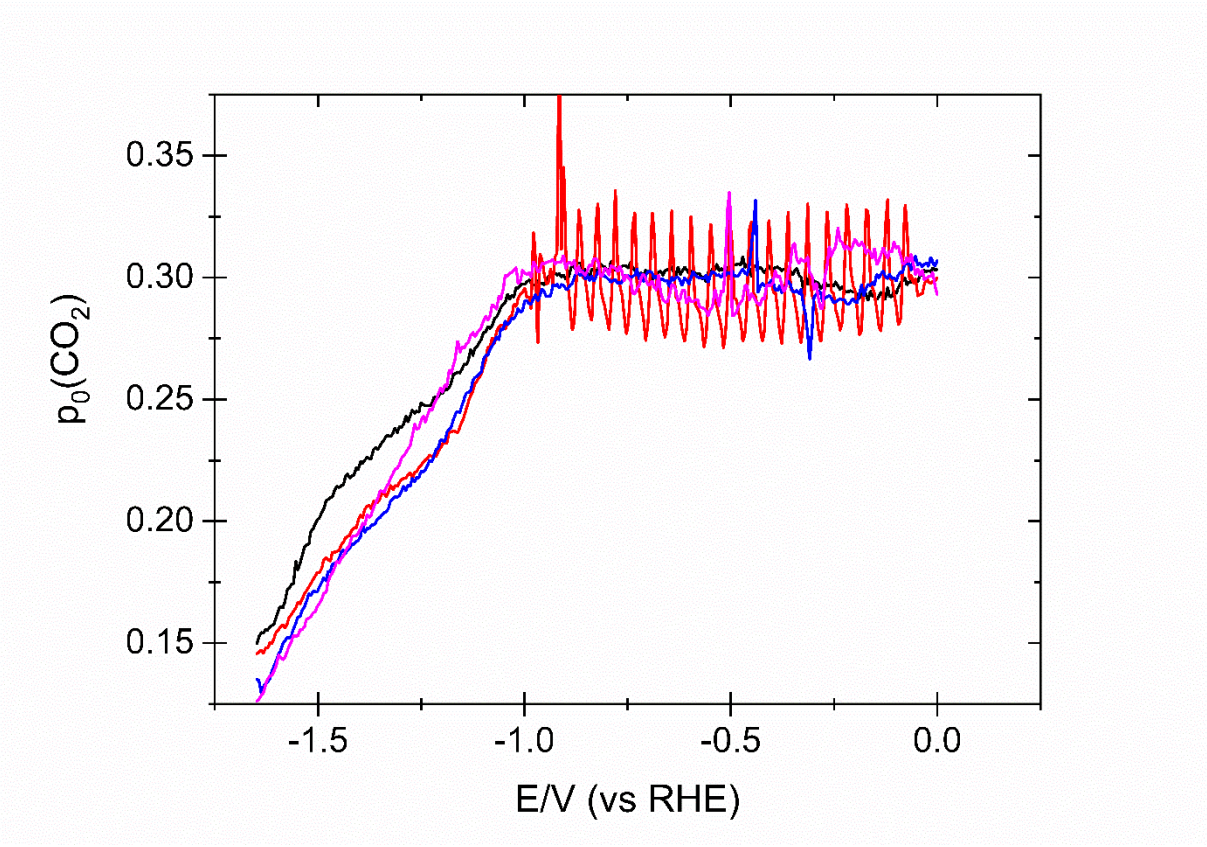

Figure S11: The CO_2 partial pressure at the electrode surface estimated from Equation S5 for the measurements shown in Figure S2. The electrolyte of 0.5 M $NaClO_4$ containing 1 mM (black), 0.63 mM (red), 0.4 mM (blue) and 0.25 mM (magenta) $HClO_4$ was purged with an Ar/CO_2 mixture featuring a CO_2 partial pressure of 0.3 bar. Working electrode: Au(pc) (roughness factor: 20.3; exposed geometric surface: area 0.283 cm^2); Sweep rate: 20 mV/s; Flow rate: 5 µL/s.

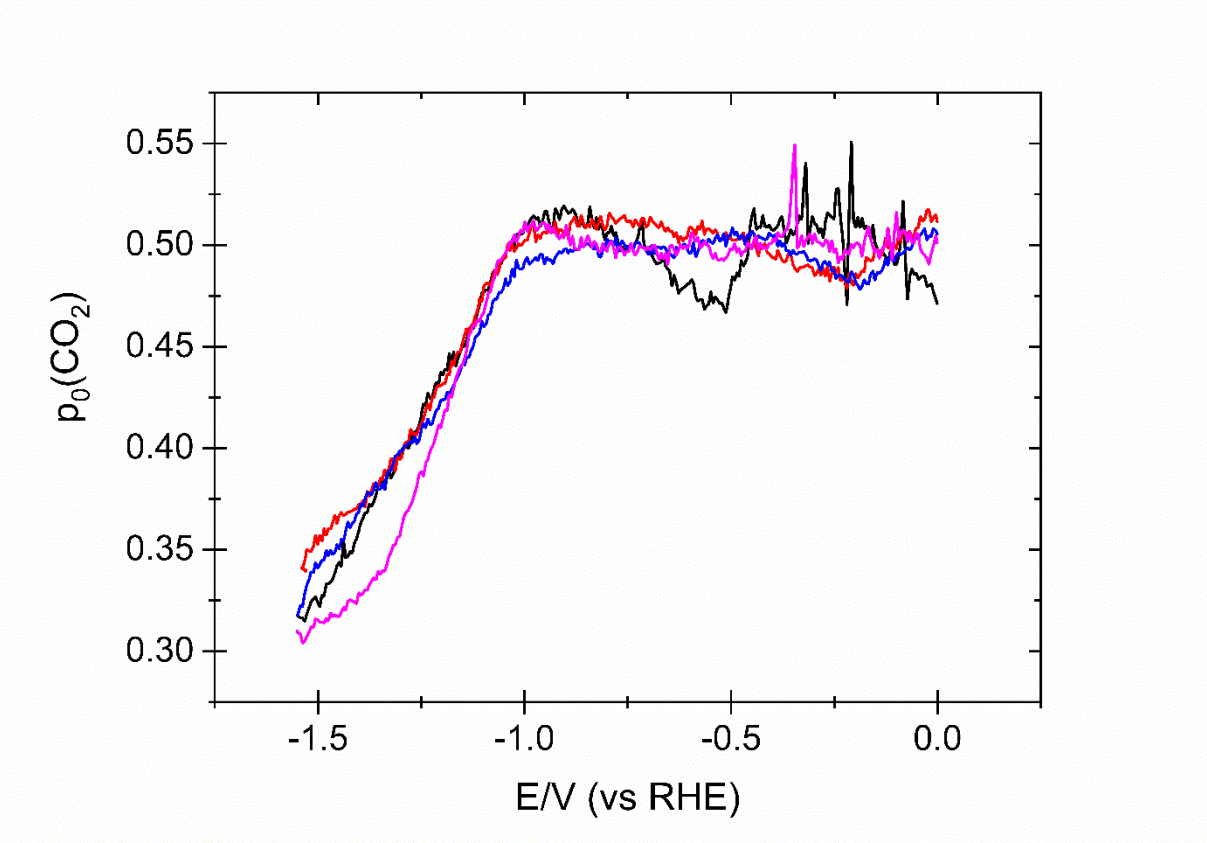

Figure S12: The CO_2 partial pressure at the electrode surface estimated from Equation S5 for the measurements shown in Figure S3. The electrolyte of 0.5 M $NaClO_4$ containing 1 mM (black), 0.63 mM (red), 0.4 mM (blue) and 0.25 mM (magenta) $HClO_4$ was purged with an Ar/CO_2 mixture featuring a CO_2 partial pressure of 0.5 bar. Working electrode: Au(pc) (roughness factor: 20.3; exposed geometric surface: area 0.283 cm^2); Sweep rate: 20 mV/s; Flow rate: 5 µL/s.

It is evident from Figure S6 that the baseline of the ionic current for mass 44 is rather unsteady. This is due to the unsteady motion of the syringe pump, with which we control the electrolyte flow through the dual thin layer cell. Small changes in the flow rate mean that also the amount of CO_2 evaporating into the mass spectrometer changes somewhat. This behavior cannot be avoided and is particularly intense when the electrolyte is purged with an Ar/CO_2 mixture featuring a high CO_2 partial pressure. Therefore, changes in the baseline render it difficult to observe slight differences in $p_0(CO_2)$ for electrolytes featuring different proton concentrations in Figures S11 and S12. However, the baseline in Figure S10 is steadier and it is possible to decern that $p_0(CO_2)$ remains highest at any potential

when the proton concentration is high as well. That is: protons keep CO_2 from reacting with OH^- and maintain therefore a higher local CO_2 concentration at the electrode surface. Therefore, we observe a slight increase of the CO formation rate in Figures S1, S2 and S3 when the proton concentration is increased. The latter do not take part in the rate determining step of CO_2 reduction[1] and should not affect the CO formation rate in a direct fashion. However, they exert an indirect effect on the local CO_2 concentration, which enters the rate law of CO_2 reduction.

References:

(1) a) Ringe, S.; Morales-Guio, C. G.; Chen, L. D.; Fields, M.; Jaramillo, T. F.; Hahn, C.; Chan, K. Double layer charging driven carbon dioxide adsorption limits the rate of electrochemical carbon dioxide reduction on Gold. *Nature communications* **2020,** *11* (1), 33; b) Shen, J.; Kortlever, R.; Kas, R.; Birdja, Y. Y.; Diaz-Morales, O.; Kwon, Y.; Ledezma-Yanez, I.; Schouten, K. J. P.; Mul, G.; Koper, M. T. M. Electrocatalytic reduction of carbon dioxide to carbon monoxide and methane at an immobilized cobalt protoporphyrin. *Nature communications* **2015,** *6*, 8177; c) Wuttig, A.; Yaguchi, M.; Motobayashi, K.; Osawa, M.; Surendranath, Y. Inhibited proton transfer enhances Au-catalyzed CO2-to-fuels selectivity. *Proceedings of the National Academy of Sciences of the United States of America* **2016,** *113* (32), E4585-93; d) Birdja, Y. Y.; Pérez-Gallent, E.; Figueiredo, M. C.; Göttle, A. J.; Calle-Vallejo, F.; Koper, M. T. M. Advances and challenges in understanding the electrocatalytic conversion of carbon dioxide to fuels. *Nat Energy* **2019,** *4* (9), 732–745;